Journal of Thermal Analysis and Calorimetry (2022) 147:11535–11547
https://doi.org/10.1007/s10973-022-11310-x

Experimental research on multistep decomposition kinetics of ammonium perchlorate in the space-confined environment

Hua-Bo Li[1] · Xiao-Qiao Zhao[1] · Wen-Qian Wu[1] · Shi-Ran Li[2] · Li-Ping Chen[1] · Wang-Hua Chen[1]

Received: 27 October 2021 / Accepted: 7 March 2022 / Published online: 3 May 2022

Abstract

The decomposition kinetic analysis of ammonium perchlorate (AP) has long been the research focus for involving various physicochemical phenomena. In this article, differential scanning calorimetry (DSC) measurements with specially made glass crucible were carried out to study the decomposition process of AP in the space-confined environment for the first time. It discovers that the peak temperature (T_{p2}) of high-temperature decomposition (HTD) and the final reaction temperature ($T_{end,D}$) shift to a lower temperature as the sample mass increased. It also indicates that such decomposition process can be deconvoluted into three reaction steps: endothermic, low-temperature decomposition, and HTD. Moreover, kinetic parameters of the reaction process were calculated via isoconversional and model fitting methods. The correctness of the fitted kinetic parameters was verified by the reconstruction of the primitive experimental curves. The obtained reaction model contributes to an improved understanding of AP's thermal decomposition in the space-confined environment.

Keywords Ammonium perchlorate · Differential scanning calorimetry · Mathematical deconvolution analysis · Isoconversion method · Model fitting method

Abbreviations

$A(\alpha)$	Pre-exponential factor, s^{-1}
A_1	Pre-exponential factor of endothermic reaction stage, s^{-1}
A_2	Pre-exponential factor of LTD reaction stage, s^{-1}
A_3	Pre-exponential factor of the HTD, s^{-1}
E_α	Apparent activation energy, kJ mol^{-1}
E_1	Apparent activation energy of endothermic reaction stage, kJ mol^{-1}
E_2	Apparent activation energy of LTD reaction stage, kJ mol^{-1}
E_3	Apparent activation energy of HTD reaction stage, kJ mol^{-1}
$F_i(t)$	The mathematical peak function
N	The total number of peaks
Q	Specific decomposition heat, J g^{-1}
R	Universal gas constant, 8.314 J mol^{-1} K^{-1}
T	Temperature, K
T_0	The temperature at which the DSC curve begins to deviate from the baseline, °C
T_{p1}	The LTD exothermic peak temperature, °C
T_{p2}	The HTD exothermic peak temperature, °C
$T_{end,\ D}$	The end reaction temperature of decomposition, °C
T_{onset}	Onset temperature of phase transition, °C
T_{end}	The end reaction temperature of phase transition, °C
T_p	Peak temperature of phase transition, °C
ΔH	The average heat production, J g^{-1}
a_0	The amplitude, mW
a_1	The position, °C
a_2	The half width, °C
a_3	The asymmetry
$f(\alpha)$	Reaction model
n_1	Reaction order of endothermic reaction stage
$n_{21,}\ n_{22}$	Reaction order of LTD reaction stage
n_3	Reaction order of HTD reaction stage
r_i	Reaction rate of the stage *i*, stage
t	Time, s
x	Arbitrary independent variable
α	Reaction progress, the extent of conversion
β	Heating rate, K s^{-1}

Hua-Bo Li and Xiao-Qiao Zhao contribute equally to the article.

✉ Li-Ping Chen
clp319@njust.edu.cn

[1] Department of Safety Engineering, School of Chemical Engineering, Nanjing University of Science and Technology, Nanjing 210094, Jiangsu, China

[2] Wanhua Chemical Group Co., Ltd, Yantai 264002, Shandong, China

Subscripts

i Reaction number

Introduction

Ammonium perchlorate (AP, NH_4ClO_4) has been widely used as a characteristic oxidizer in various composite solid propellants (CSPs) and pyrotechnics due to its higher oxidation potential, positive oxygen balance, and excellent compatibility with other solid propellant components [1]. Several thermal decomposition characteristic parameters of AP, such as burning rate, the temperature of high-temperature decomposition (HTD), and activation energy, play a remarkable role in the combustion/explosion behavior of CSPs, which makes AP attract much more attention during the past decades [2, 3]. However, the presence of chlorine element in the molecule makes AP's decomposition process fundamentally different from other oxidizer and explosive substances. Furthermore, the experimental conditions, crystal history, presence of defects or impurities are also pivotal to the decomposition rate and combustion behavior of AP [4], which makes the decomposition of AP rather more complicated. Some of the problems are still unsolved.

Up to now, a large number of research works have been reported on AP. However, most of them focused on the decomposition mechanism and structural properties of AP; only a small number of scholars investigated the thermal decomposition kinetics. Lang and Sergey Vyazovkin [5] examined the decomposition characteristic of AP under different sample types by thermogravimetric (TG) and differential scanning calorimetry (DSC). The effective activation energy is determined by the isoconversional kinetic analysis. Yan-Li Zhu et al. [6] obtained the nonisothermal data of AP at different heating rates by TG/DSC analysis. The kinetic parameters were calculated by multivariate nonlinear regression. Rajić and Sućeska [7] studied the decomposition kinetics of AP at low temperatures by the isothermal thermogravimetric method. The kinetic Eq. (1) used in their work was initially developed to describe the process of nucleation and linear growth of nuclei. But Rajić and Sućeska found this equation could also describe the thermal decomposition of AP at their tested temperature range. Sergey Vyazovkin and Charles A. Wight [8] studied the thermal decomposition of cubic AP by TGA/DSC. Based on the isothermal and nonisothermal data, the relationship between the activation energy and conversion was established.

$$\frac{d\alpha}{dt} = k\alpha^{n}(1-\alpha)^{m} \tag{1}$$

It is worth noting that the decomposition kinetics analysis of AP reported in the above works is based on the isoconversional method. This method can't determine the actual reaction model. In addition, when conducting the thermal analysis experiments about AP, most of the reported works used the metal crucible with no lid or pierced lid, which made the intermediate gaseous products escape from the crucible easily and further led to various different experiment results [3, 5, 9–13]. In practice, AP was commonly used in a space-confined environment. The intermediate gaseous decomposition products are not escaped. Thus, AP's decomposition process in the space-confined environment is different and more complicated than that in an open environment. To our best knowledge, no work about the decomposition of AP in the space-confined environment has been reported. In addition, the decomposition of AP is highly sensitive to some additives, such as metals, metal alloys, and their oxides, notably the transition metals [10, 14, 15]. In practice, most of the crucibles are made of stainless steel or alloy materials, which cannot meet the inertness relationship between the crucible and sample as AP could react with the crucible material. Therefore, the selection of crucible is crucially important in thermal analysis, which is often ignored in the experiment. It's necessary to investigate thermal behavior characteristics and the decomposition kinetic model of AP in the space-confined environment with no catalytic material existing.

In the present study, the decomposition characteristic of AP in the space-confined environment was studied under different test condition. The mathematical deconvolution analysis (MDA) was utilized to separate the decomposition peak according to the actual reaction process. At last, the model kinetic reaction was evaluated by isoconversional and nonlinear optimization methods. The obtained kinetic information is vitally important to predict the thermal stability of various CSPs containing AP under different thermal stress during handling and storage.

Experiment and method

Sample

AP (purity above 98.8%), in the form of a white crystal, with an average particle size of 250–425 μm, was used in the research. The sample was stored in desiccator with silica-gel drier to prevent absorption of moisture and degradation and used directly without any processing or purification.

DSC test

All experiments were conducted on the heat flow-type differential scanning calorimeter (DSC-1) manufactured by the METTLER TOLEDO, Switzerland. To ensure an analogous test environment, the test was implemented in a high-purity nitrogen atmosphere (99.999%) with a flow rate of 50 mL min^{-1}.

DSC test with different crucibles

The metal crucibles of commonly used stainless, silver-plated, gold-plated, and inert glass crucible were used to conduct the dynamic DSC experiment with heating rate of 8 K min^{-1}. The sample was all located in a space-confined environment. The metal crucibles were directly bought from the franchiser, but the glass crucible was specially manmade. The specific manufacturing process is as follows: firstly, the sample was loaded in a glass crucible (directly bought from the Duran company) with an internal diameter of 1 mm, a wall thickness of 0.25 mm, and a length of about 15 mm. The crucible was sealed by a high-temperature flame after loading the sample. At last, silver foil wrapped around the outside of crucible to reduce the heat resistance between the crucible and DSC sensor [16]. The sample in the metal crucibles was also sealed with a lid closed on, which can sustain a pressure of about 15 MPa. The sample mass is about (0.75 ± 0.01) mg.

DSC test with the glass crucible

Due to the higher energetic nature and larger gas production of such a material, a small sample mass, less than 1 mg, was used for the test to avoid the larger self-heating rate and pressure effect [17]. First of all, different mass of AP was screened at 8 K min^{-1} to research the influence of mass on the decomposition characteristics of the sample. Then, about (0.61 ± 0.01) mg of sample was screened from 200 to 450 °C at different heating rates of 4, 8, 10, 15 K min^{-1}, respectively. To identify the autocatalytic of the sample, the isothermal DSC test at 260 °C was also conducted. The experiments were all carried twice with similar initial masses to ensure the repeatability and reproducibility of experimental data.

Table 1 Thermal decomposition characteristic parameters of AP with different crucibles

Type of crucible	M/mg	T_0/°C	T_{end}/°C	ΔH/ J g^{-1}
Stainless steel crucible	0.76	308.72	440.20	−3171.44
Gold-plated crucible	0.75	283.38	401.61	−8786.84
Silver-plated crucible	0.76	271.11	426.55	−2985.62
Glass crucible	0.75	280.78	347.35	−1593.17

T_0 is the temperature at which the DSC curve begins to deviate from the baseline; T_{end} is the end reaction temperature of decomposition reaction process

At the end of each test, the glass crucible was reweighed to examine the mass loss during the experiment. All the experimental curves were obtained after baseline correction by the advanced thermal safety software.

Results and discussion

Decomposition characteristics of AP at different crucibles

As a strong oxidant, AP generates different types of strong oxidative and acidic gases during decomposition. Some metal materials of the crucible may affect the decomposition process of AP. Figure 1 shows different heat flow curves of AP with different crucibles, and the corresponding core parameters of the thermal decomposition are listed in Table 1. The crystal transformation process didn't show in the figure as the relatively low heat flow value.

As shown in Fig. 1, it has an entirely different heat flow curves as AP is located in different crucibles. The specific heat production in the metal crucible is obviously greater

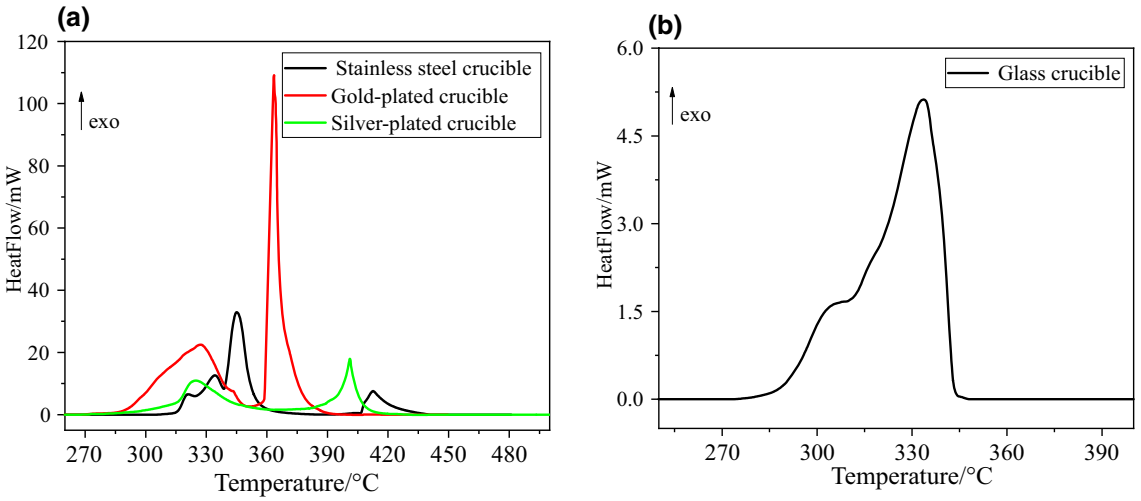

Fig. 1 DSC curves of AP with different crucibles. **a** Common used metal crucibles; **b** inert glass crucible

than that of in the glass crucible, especially in the gold-plated crucible, which is more than 5 times than that of in the glass crucible. The higher exothermic heat in the metal crucible was caused by the interactivity of AP with the metal crucible used in the DSC test, as the transition metals could greatly change the proton concentration in the lattice during the decomposition process [10, 14, 15]. Just because of this, the glass crucible is used in the following analysis.

Influence of sample mass on the decomposition characteristics of AP

To determine the effect of sample mass on the decomposition of AP in the space-confined system, a series of DSC screening tests at 8 K min^{-1} were carried out with the sealed glass crucible. The sample mass ranges from 0.20 to 0.60 mg. Figure 2 shows the heat flow results of AP under different sample masses; the corresponding thermal decomposition parameters are summarized in Table 2.

As shown in Fig. 2, AP undergoes one endothermic crystal transformation process and two consecutive exothermic processes. The crystal transformation takes place at the temperature range from 240 to 245 °C with the transition enthalpy of 73.34 ± 2.83 J g^{-1}, which is in line with the results in Refs. [18–20]. At the low-temperature decomposition (LTD) process, the sample decomposes at 278.57 ± 3.30 °C (T_0) with the peak temperature of 304.26 ± 2.14 °C (T_{p1}). Obviously, the sample mass hardly affected the crystal transformation process and the LTD process. However, the peak temperature (T_{p2}) and the final reaction temperature ($T_{end,\ D}$) of the HTD process shift to a lower temperature with the sample mass increased. The findings indicate that the observed forward HTD reaction could be attributed to the increased sample mass. According to the previous research, the final decomposition products of AP are a mixture of various gas species, such as O_2, Cl_2, N_2O, NO_2, HNO_3, H_2O, HCl, ClO, and HOCl [21]. As the sample mass increased, more gaseous products could gather in the sealed glass crucible with constant volume, which gives rise to the higher pressure in the crucible. Eventually high pressure may cause the change from a high-temperature reaction zone to a lower temperature zone. Therefore, the high gaseous product pressure may promote the decomposition of HTD.

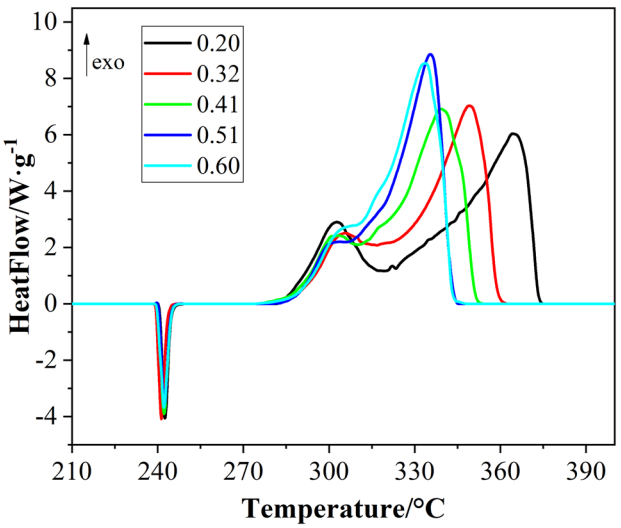

Fig. 2 DSC curves with different mass of AP at 8 K min^{-1}

Dynamic and isothermal DSC tests of AP

To study the exothermic decomposition characteristics and thermal hazards of AP, dynamic and isothermal DSC experiments with a sample mass of 0.6 mg were conducted. Figure 3 shows the heat flow curves of dynamic DSC tests at 4, 8, 10, and 15 K min^{-1}. The corresponding characteristic parameters are summarized in Table 3.

Figure 3 shows that AP undergoes the crystal transformation from the orthorhombic to cubic at the temperature of 240.50–245.00 °C, and an exothermic process starts at about 260.87–289.53 °C (T_0). The exothermic process includes two steps. The first is from 289.53 °C to approximately 318.58 °C (for 15 K min^{-1}); the second is from 318.58 °C to approximately 364.71 °C (for 15 K min^{-1}). Additionally, the T_{p2}, and $T_{end,\ D}$ are lower than that of Refs. [6, 21]. The

Table 2 Thermal decomposition characteristic parameters of AP under different mass

M/mg	Crystal transformation process				Decomposition reaction process				
	T_{onset} /°C	T_p /°C	$T_{end,\ C}$ /°C	ΔH /J g^{-1}	T_0 /°C	T_{p1} /°C	T_{p2} /°C	$T_{end,\ D}$ /°C	ΔH /J g^{-1}
0.20	240.74	242.54	244.60	74.06	281.87	302.67	364.35	374.84	−1718.00
0.32	241.42	243.27	245.82	73.05	278.63	302.12	351.15	367.07	−1652.59
0.41	240.98	243.00	245.53	70.59	275.27	305.00	347.81	361.05	−1687.57
0.51	240.90	242.65	245.30	70.50	279.48	305.23	334.75	349.06	−1586.01
0.60	239.79	242.24	244.82	76.17	280.78	306.39	333.65	347.35	−1613.17

T_0 is the temperature at which the DSC curve begins to deviate from the baseline; T_{p1} is the LTD exothermic peak temperature; T_{p2} is the HTD exothermic peak temperature; $T_{end,\ C}$ and $T_{end,\ D}$ are the end reaction temperature of crystal transformation process and decomposition reaction process

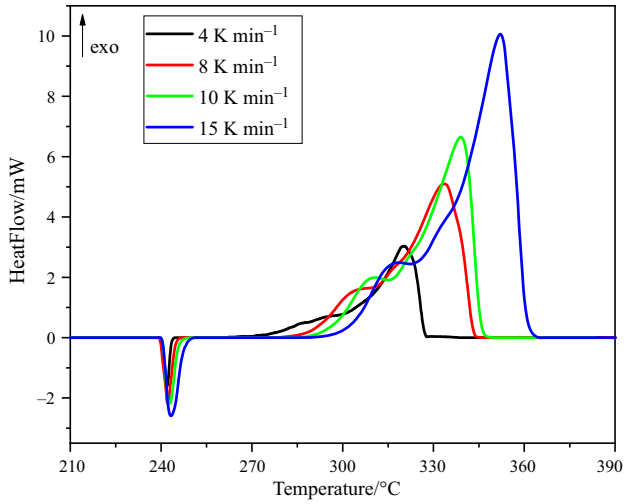

Fig. 3 Dynamic DSC curves of AP at heating rate of 4, 8, 10, and 15 K min^{-1}

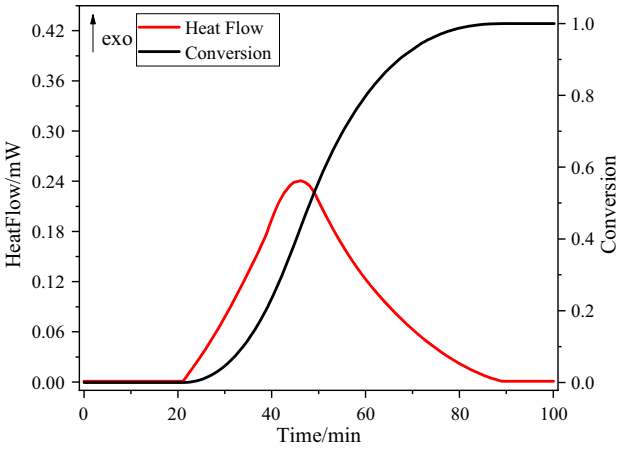

Fig. 4 Isothermal DSC curves of heat flow and conversion *vs*. time for AP at 260 °C

average heat production is 1526.39 J g^{-1}, which is higher than the results in Ref. [8, 22, 23]. According to the Zurich hazard analysis method (Z-H-A) developed by Zurich Insurance Company [24], it will cause catastrophic consequences once the runaway reaction occurs.

As mentioned in Ref. [5, 10, 25–27], the LTD process of AP usually follows the autocatalytic decomposition mechanism. In order to verify this statement, the isothermal DSC test at 260 °C was conducted. The result is shown in Fig. 4.

According to ICTAC, the numerous reaction models can be summarized into three major types: decelerating, accelerating, and sigmoidal (also called autocatalytic) [28]. Each type has its own representative curve characteristics. As shown in Fig. 4, one exothermic peak is detected at the selected setting temperature. The heat flow reaches its peak (0.2404 mW) at 46.27 min. The correlation between the conversion and time is also displayed in Fig. 4. The curve shows an evident accelerating and decelerating behavior in the initial and final stages. Therefore, the LTD process of AP is an autocatalytic reaction.

However, the total heat generation of the isothermal test is about 744.20 J g^{-1}, which is much lower than the dynamic DSC results in Table 3. A white porous residue remained at the end of the isothermal experiment, which indicates the decomposition of AP may be incomplete. In order to verify this conjecture, an additional dynamic experiment of 8 K min^{-1} was carried out on the residue and compared with the original DSC curve of 8 K min^{-1} in Fig. 3. The results are shown in Fig. 5.

As shown in Fig. 5, both the original AP and residue presented an endothermic process at about 242°C. The endothermic heat of residue is about 32.61 J g^{-1}, which is significantly lower than the transition enthalpy of AP. In addition, the original AP underwent a multi-steps exothermic process while the residue only presented one exothermic peak. The decomposition enthalpy for residue is about 828.33 J g^{-1}, which is close to the heat difference between the non-isothermal experiment (1613.17 J g^{-1}) and the isothermal experiment (744.20 J g^{-1}). For the residue decomposition, the LTD is suppressed and the decomposition mainly takes place at the high temperature.

Peak separation by mathematical deconvolution analysis

Review of previous work about reaction process of AP

The thermal decomposition process of AP has been widely accepted to be an intricate solid–gas-phase reaction process dominated by miscellaneous physicochemical phenomena,

Table 3 Thermal decomposition characteristic parameters of AP in the dynamic DSC test

β /K min^{-1}	M /mg	Crystal transformation process			Decomposition reaction process				
		T_{onset} /°C	T_p /°C	ΔH /J g^{-1}	T_0 /°C	T_{p1} /°C	T_{p2} /°C	$T_{end,D}$ /°C	ΔH /J g^{-1}
4	0.60	240.35	242.02	73.95	260.87	296.60	320.38	328.62	−1505.37
8	0.60	239.78	244.83	77.25	277.45	307.82	333.65	345.75	−1613.17
10	0.61	240.48	245.68	72.68	285.83	310.53	338.98	349.61	−1471.95
15	0.61	240.45	243.26	78.10	289.53	318.58	352.01	364.71	−1515.06

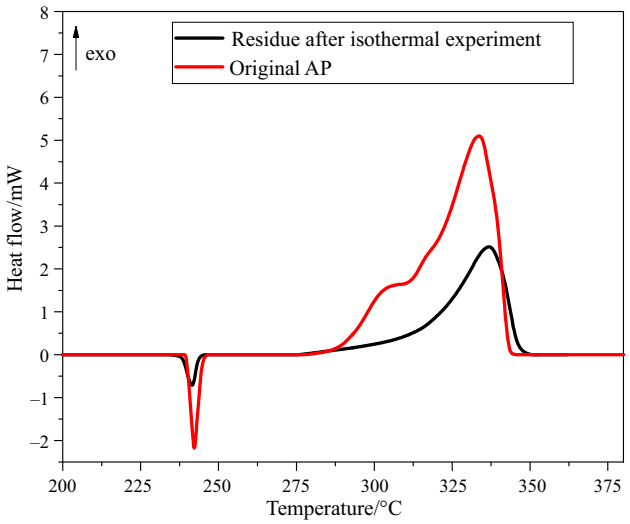

Fig. 5 DSC curve comparison diagram between the original AP and the residue at 8 K min^{-1}

such as crystal transformation, sublimation, diffusion, adsorption–desorption [25, 29, 30]. The possible reaction pathways for the decomposition of AP are illustrated schematically in Fig. 6. Firstly, it experiences a reversible crystallographic transition process from the orthorhombic structure to the cubic one with an endothermic peak at 240–245 °C as shown in the green part in Fig. 6. The crystal transformation heat is about 11.3 kJ mol^{-1} [31].

Dodé first recorded that the sublimation of AP is the principal factor with the essentially endothermic nature [25]. In this stage, AP experiences proton transfer to form a molecular complex of NH_3 and $HOClO_3$ in the relaxed surface layer; then, the molecular complex dissociates to ammonia and perchloric acid in the gas phase [32] as illustrated in the red part in Fig. 6. Bircumshaw and Newman [33] discovered that the process of decomposition and sublimation proceeds instantaneously throughout the whole decomposition process. The particular nature of the endothermic peak in the curve is the competition result between the endothermic sublimation process and the exothermic thermal decomposition process [5, 8]. The sublimation of AP is highly dependent on the sample topography and the applied pressure [5].

The escape of the sublimation products is hindered by the limited conditions. The sublimation products may be adsorbed on the surface of the crystal or react with each other in the gas phase, which induces a remarkable exothermic effect. In the exothermic chemical reaction process, most of the researchers support a two-step kinetic model, LTD and HTD, based on the decomposition temperature from the thermal analysis [25, 29, 34]. The LTD is ascribed to the partial decomposition of AP and is ceased after about 30% decomposition, while the HTD is ascribed to the decomposition of intermediate products into volatile products.

At the very beginning of LTD, the decomposition/sublimation products (ammonia and perchloric acid) are adsorbed in the crystal lattice defect site, which is located in pores just below the crystal surfaces about several micrometers [35]. Once a crystal reaction center is activated, the reaction nuclei begin to form and grow, and then merge to form the reaction region. Owing to the interaction of stresses, strains, and reactant consumption, this process exhibits an induction period, and AP undergoes an autocatalytic reaction. The Avrami Erofeev and Prout Tompkins equations are most frequently applied to analyze kinetic data [5, 25–27]. The rate of ammonia outflow from a pore is about 2.5 times higher than that of perchloric acid [3, 14, 34]. The ratio of ammonia to perchloric acid decreases continuously in reaction nuclei. Therefore, the perchloric acid's accumulation will induce the proton equilibrium equation to shift to the left-hand side [3]. Furthermore, the oxidation of ammonia turns incomplete; the surface is covered with ammonia [34]. Those factors are responsible for the incomplete transformation of perchlorate and the cessation of the reaction, leaving a porous residue that is indistinguishable from the primeval substance composition [33, 35].

The situation undergoes some changes when a higher temperature is introduced. Under such a circumstance, the proton transfer from NH_4^+ to ClO_4^- firstly proceed; then, the adsorption and desorption phenomenon of ammonia and perchloric acid takes place on the surface of the crystal; at last, the secondary reactions between the thermal decomposition products occur either on the surface of AP or in the gas phase above the surface under suitable conditions [22, 34]. It should be noted that the shape of the DSC curve at high temperature depends strongly on the testing conditions. If the experiment runs in an opened sample pan with a lower heating rate, an endothermic peak may occur [5, 8, 10, 36].

Peak separation results

According to the dynamic DSC experiments curves shown in Fig. 3, the decomposition of AP is a multi-step process [37]. These overlapped heat flow peaks should be separated from each other to be helpful for kinetics analysis. In this paper, mathematical deconvolution analysis (MDA) is used to achieve this goal. Its basic idea is to fit overlapped peak with the mathematical functions $F(t)$ as follows:

$$\frac{d\alpha}{dt} = \sum_{i=1}^{N} F_i(t) \tag{2}$$

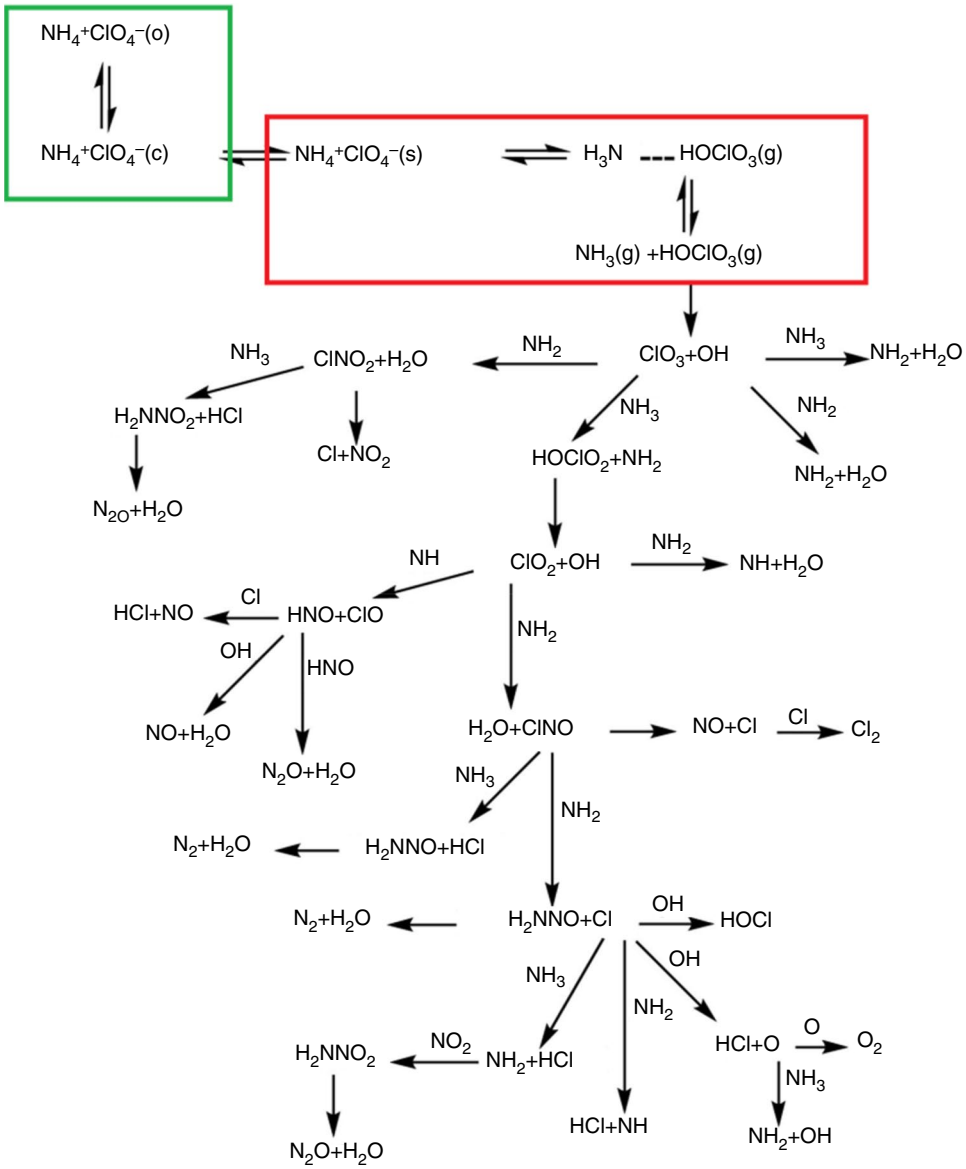

Fig. 6 Diagrammatical illustration of the possible reaction pathways about the decomposition of AP [32, 45, 46]. Note: (o) refers to NH_4ClO_4 in the orthorhombic structure, **c** refers to NH_4ClO_4 in the cubic structure, (s) refers to the relaxed surface, and (g) refers to the gas phase

$$F(t) = a_0 \exp\left[-\ln 2\left[\frac{\ln\left(1+2a_3\frac{x-a_1}{a_2}\right)}{a_3}\right]^2\right] \quad (3)$$

where $F_i(t)$ is the mathematical peak function, N is the total peaks number, a_0 is the amplitude, a_1 is the position, a_2 is the half-width, and a_3 is the asymmetry. x indicates an arbitrary independent variable. This method could fit not merely ideal kinetic model curves but also the kinetic curves whose model diverges from the ideal ones for the reason of heterogeneities in particle size or shape [38]. This method has been used widely in the kinetic analysis of complex solid-state reactions, such as ammonium dinitramide, 2,6-diamino-3,5-dinitropyrazine-1-oxide (LLM-105), co-precipitated zinc carbonates, poly(vinyl chloride) (PVC), tin(II) oxyhydroxide, and *trans*-bis(ethylenediamine) cobalt (III) hexafluorophosphate [39–44].

From the analysis in Sect. 3.4.1, it is clear that the first decomposition stage of AP is sublimation to NH_3 and $HClO_4$ by proton transfer. Furthermore, the cleavage of the HO−ClO_3 bond is also an early key step [45], for the ClO_3^- is an efficient proton trap during the proton transfer from the ammonium ion to perchlorate. Both of those processes are endothermic [5, 32, 45, 46] and could be characterized by Nth order [47–49]. Therefore, they could be merged into one process. The value of endothermic heat cannot be obtained directly from the DSC curves, but could be captured from some literature. Based on Ref. [32, 45], the enthalpy change for the sublimation reaction is about 1600.98 J g^{-1}, and that of the HO–ClO_3 bond cleavage reaction is about 1536.94 J g^{-1}. The total endothermic heat is

3137.92 J g^{-1}. Besides, the appearance of two shoulders in the exothermic peak means the decomposition comprises two reaction processes. Consequently, according to the reaction mechanism and reaction temperature, the exothermic decomposition could be divided into three stages, endothermic (P1), LTD (P2), and HTD (P3) stage.

Figure 7 shows the comparison between experiments and simulations of heat flow for AP. The simulated line (red line) is coincident with the experimental one (triangle scatter dot with black). The fitted model parameters of the separated peaks are shown in Table 4. The negative heat flow curves (blue line) manifest an endothermic process owed to the sublimation of AP and the cleavage of the HO–ClO_3 bond. The contribution of the endothermic stage is practically negligible at lower conversion, but increases significantly during decomposition. This finding is in line with that found in [8]. The positive value of heat flow manifests that the exothermic reaction is owed to the LTD and HTD.

Activation energy analysis based on the isoconversional method

The isoconversional methods could determine the activation energy in the absence of the mechanism function. This method is often used as an optimal choice for acquiring mechanism model or affording initial guesses for model fitting methods [28]. Considering the Arrhenius expression, the activation energy can be determined by the logarithmic derivative of the reaction rate at a particular conversion:

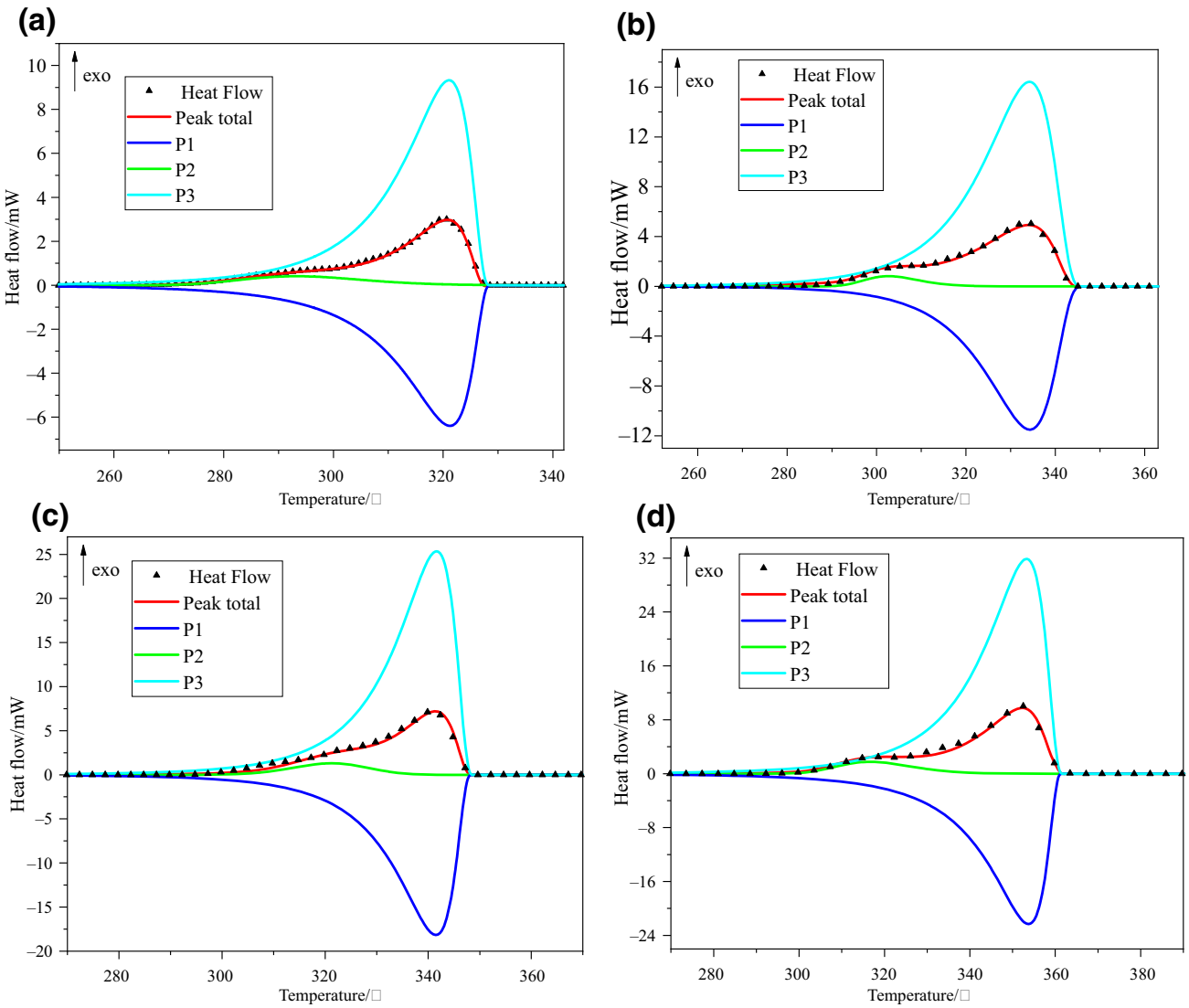

Fig. 7 Peak separation results of AP under the heating rate of 4 (**a**), 8 (**b**), 10 (**c**), 15 K min^{-1} (**d**). Note: P1 is the endothermic reaction stage, P2 is the LTD reaction stage, and P3 is the HTD reaction stage

Table 4 Peak separation parameters of AP under different heating rates

Peak	a_0 /mW	a_1 /°C	a_2 /°C	a_3	Q /mJ	Peak	a_0 /mW	a_1 /°C	a_2 /°C	a_3	Q /mJ
4-P1	−6.39	321.26	13.55	−0.89	−1842.95	8-P1	−11.50	334.31	17.15	−0.70	−1856.26
4-P2	0.41	293.27	25.79	0.16	128.77	8-P2	0.82	302.67	14.00	0.22	135.00
4-P3	9.33	321.10	13.09	−0.85	2617.46	8-P3	16.42	334.22	17.52	−0.70	2689.90
10-P1	−18.18	341.49	12.27	−0.85	−1856.45	15-P1	−22.31	353.72	14.47	−0.91	−1855.55
10-P2	1.31	321.29	17.06	−0.09	133.45	15-P2	1.77	316.68	20.33	0.20	131.02
10-P3	25.37	341.46	12.23	−0.84	2620.61	15-P3	31.87	353.26	15.02	−0.85	2648.29

$$\ln\left(\beta\frac{\mathrm{d}\alpha}{\mathrm{d}T}\right)=\ln\left[A(\alpha)f(\alpha)\right]-E_\alpha/RT \tag{4}$$

where α is the conversion; β is the heating rate, K s^{-1}; T is the absolute temperature, K; E_α is the activation energy at α, kJ mol^{-1}; $f(\alpha)$ is the kinetic model function; R is the universal gas constant, kJ mol^{-1} K^{-1}; $A(\alpha)$ is the pre-exponential factor at α, s^{-1}. The correlation between $\ln[\beta(\mathrm{d}\alpha/\mathrm{d}T)]$ and $1/T$ shows a straight line with the intercept of $\ln[A(\alpha)f(\alpha)]$ and the slope of $(-E/R)$. Therefore, E and $\ln[\beta(\mathrm{d}\alpha/\mathrm{d}T)]$ at different conversion could be predicted by linear fitting methods. If E_α remains approximately constant throughout the whole reaction process, the reaction can be described by a single-step reaction model; otherwise, the reaction is kinetically complex.

The dependence of E_α, $\ln[A(\alpha)f(\alpha)]$ on α over the entire reaction process and each separated peak is shown in Fig. 8. As the initial and termination stages could be significantly fluctuated by the device noise and the baseline selection, the reaction model at the initial and termination

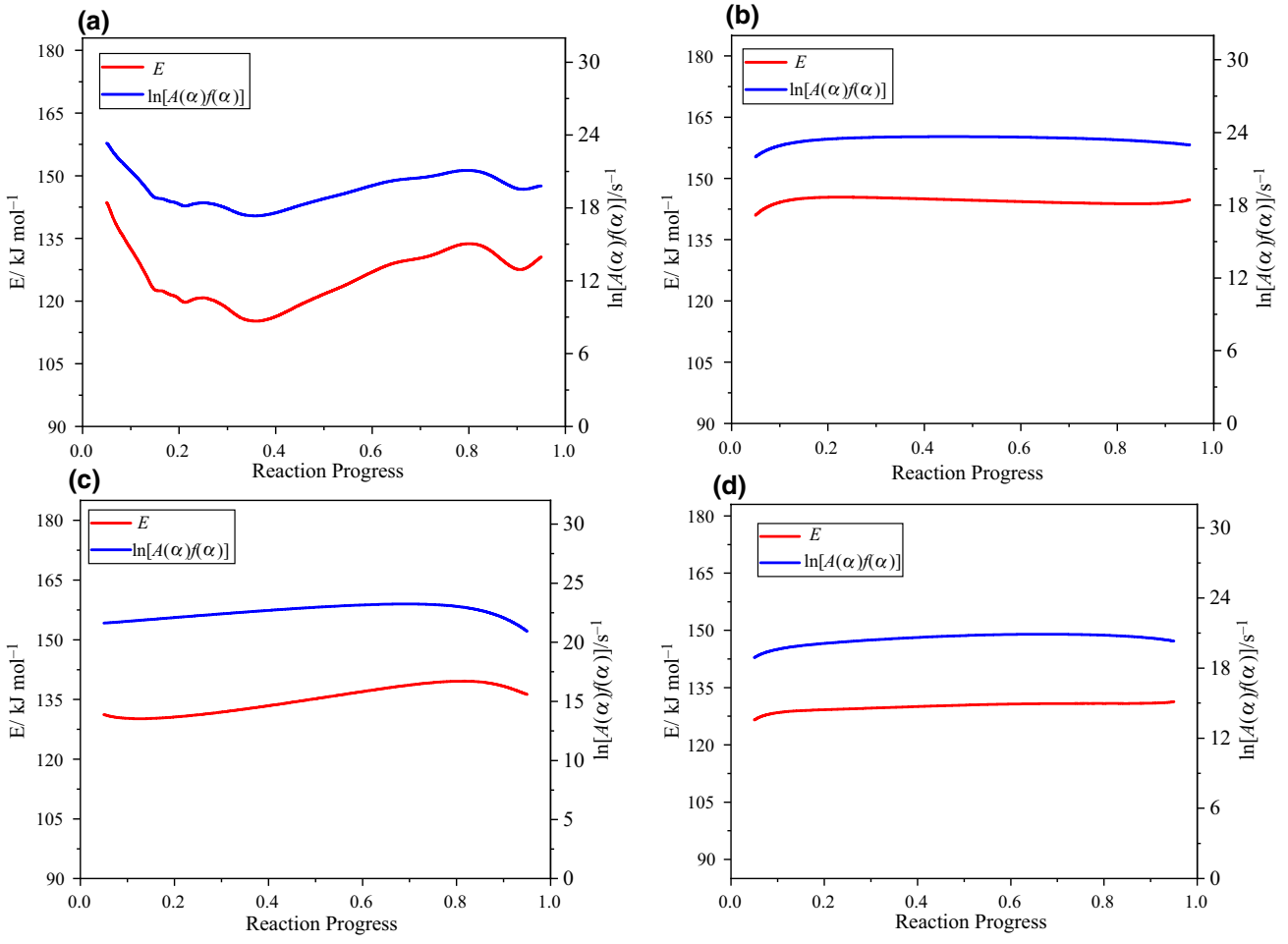

Fig. 8 Activation energy, $\ln[A(\alpha)f(\alpha)]$ versus conversion by isoconversion method. **a** Whole reaction stage, **b** endothermic reaction stage, **c** LTD reaction stage, **d** HTD reaction stage

stages is varying remarkably from the primary reaction. Hence, only E_α within the conversions range of 0.1–0.9 is effective to analyze the reaction model. The whole reaction stage (Fig. 8a) has a similar E_α variation behavior as the conversion advances reported in Ref. [8]. The E_α dependence within the conversions range of 0.1–0.9 can be divided into two stages. The first stage ($\alpha < 0.36$) corresponds to the LTD process, with the characteristics of the activation energy decreasing from 143.60 to 115.21 kJ mol^{-1}. The minimum activation energy is identified at the end of the LTD process [5, 6, 8]. The decrease in the activation energy was attributed to the development of porous structures throughout the crystals' macrostructure. The second stage ($\alpha > 0.36$) is correlated with the HTD process, which is characterized by an increase to achieve a plateau (133.72 kJ mol^{-1}) and then decrease to a minimum (127.56 kJ mol^{-1}). The above results indicate that the decomposition of AP is a complex process.

Figure 8b–d shows the E_α dependence for endothermic, LTD, and HTD stages, respectively. One can see that the variation in E_α for these stages is small. The E_α for these three stages is 143.18 ± 2.21, 134.90 ± 4.72, and 128.93 ± 2.41 kJ mol^{-1}, respectively. All of the three stages have a similar E_α, which is consistent with the conclusion of Jacobs [50], who found the activation energies for sublimation, LTD, and HTD have the same value of 125.57 kJ mol^{-1}. Because the E_α variation for each separated stage is less than 4% and could be recognized practically independent of conversion, each process can be described by a single-step reaction model.

Kinetic calculation based on the model fitting method

The reaction kinetic model plays a key role in the fields of materials development, product management, and reaction hazards assessment. Therefore, it is necessary to develop a detailed decomposition kinetic model for the decomposition process of AP.

The LTD process, which occurs in sub-surface pores, is dominated by the formation and growth of nuclei, the adsorption of ammonia and perchloric acid, and follows the autocatalytic solid–gas mechanism [10]. The Avrami Erofeev and Prout Tompkins equations are frequently applied to depict this process. Herein, the modified topochemical model in Eq. 6 was used to describe the process of LTD. The endothermic and HTD stages don't exhibit autocatalytic behavior [7]. Thus, the Nth-order kinetic model could be used to model these two stages [8].

$$\text{Endothermic reaction stage}: r_1 = A_1 \exp(-E_1/RT)(1-\alpha)^{n1} \tag{5}$$

$$\text{LTD reaction stage}: r_2 = A_2 \exp(-E_2/RT)(1-\alpha)^{n21}[-\ln(1-\alpha)]^{n22} \tag{6}$$

$$\text{HTD reaction stage}: r_3 = A_3 \exp(-E_3/RT)(1-\alpha)^{n3} \tag{7}$$

where r_1, r_2, r_3 represent the reaction rate at the endothermic, LTD, and HTD stage, respectively.

On the basis of the detailed reaction scheme and each established kinetic model, the reaction kinetic model of AP was constructed as three pathways. The scheme can be described as:

$$A \xrightarrow{r_1} B \xrightarrow{r_2} C \xrightarrow{r_3} D \tag{8}$$

$$\frac{d\alpha_1}{dt} = A_1 \exp(-E_1/RT)(1-\alpha_1)^{n1} \tag{9}$$

$$\frac{d\alpha_2}{dt} = A_2 \exp(-E_2/RT)\alpha_2^{n21}\left[-\ln\alpha_2\right]^{n22} \tag{10}$$

$$\frac{d\alpha_3}{dt} = A_3 \exp(-E_3/RT)\alpha_3^{n3} \tag{11}$$

$$\frac{dQ}{dt} = \sum Q_i \frac{d\alpha_i}{dt} \tag{12}$$

where α_1, α_2, α_3 represent the conversion rate of reactant *A* and intermediate products *B, C*, respectively. Subscript *i* represents the number of reaction stages.

Based on the above reaction model, the detailed kinetic parameters could be obtained using the nonlinear optimization method. Figure 9 shows the simulated and experimental comparison of the heat production and heat production rate profiles. The simulated profiles are in good agreement with the experimental ones, indicating that the selected reaction model is suitable to describe the decomposition process of AP in a space-confined environment. The corresponding kinetic parameters of the reaction model are listed in Table 5.

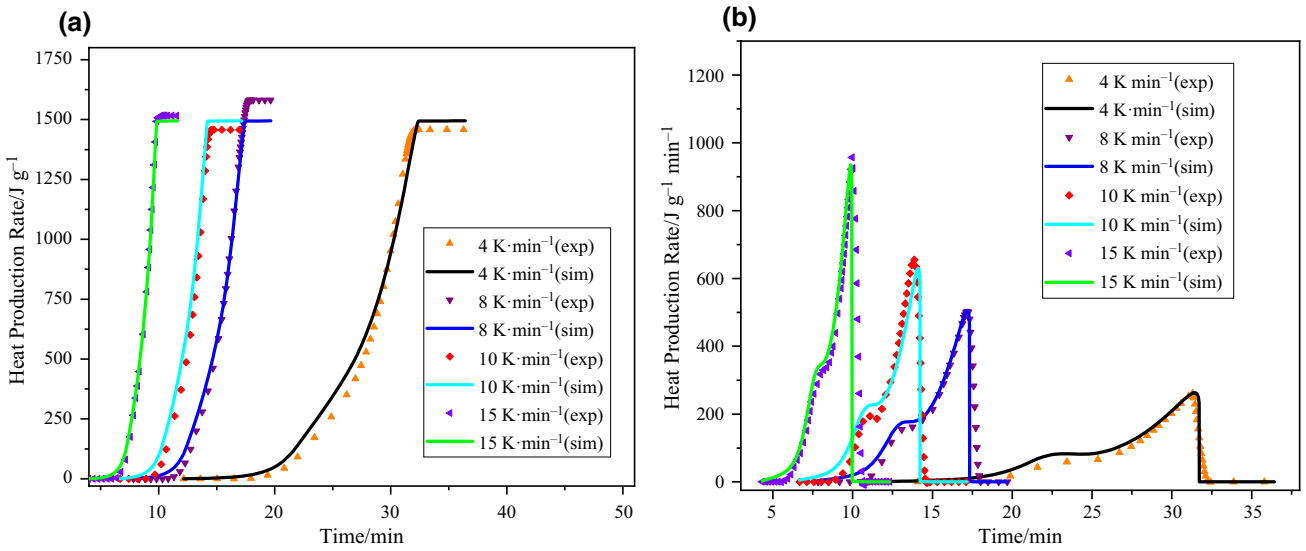

Fig. 9 Experimental and reconstructed curves of heat production *vs*. time **a** and heat production rate vs. time **b** for the whole reaction stage

Table 5 Kinetic parameters of the decomposition model for AP

Parameters	Units	Endothermic stage	LTD	HTD
ln(A)	ln(s^{-1})	32.49 ± 0.12	24.99 ± 0.36	30.73 ± 0.36
E	kJ mol^{-1}	186.22 ± 2.55	136.52 ± 1.68	172.48 ± 1.68
n_1	–	0.144 ± 0.005	–	–
n_{21}	–	–	1.65 ± 0.019	–
n_{22}	–	–	0.768 ± 0.014	–
n_3	–	–	–	0.395 ± 0.014
Q	J g^{-1}	−3115.27 ± 43.91	224.04 ± 2.58	4388.57 ± 66.21

Conclusions

In this article, DSC measurements with specially made glass crucible were carried out to study the decomposition process of AP in the space-confined environment. The AP decomposition process could be divided into three stages: endothermic reaction stage, LTD stage, and HTD stage. The MDA method was used to separate the complex solid-state reaction process into individual processes. Both the isoconversional method and model fitting method were applied to calculate the kinetic parameters. The reaction model and kinetic parameters contribute to the safety control in AP's transportation, storage as well as accident prevention. The conclusions can be summarized as follows:

(1) The metal crucible material and the sample mass could affect the decomposition process.
(2) According to the dynamic DSC curves, AP decomposes at 260.87–289.53 °C with two exothermic peaks. The average heat production is 1526.39 J g^{-1}.
(3) According to the isothermal experiment results at 260 °C, the "bell" shape in the heat flow indicates AP's decomposition is an autocatalytic reaction at the LTD stage.
(4) The partially overlapping exothermic process presented in the DSC curve was separated into three individual stages: endothermic, LTD, and HTD stages by MDA.
(5) Based on the isoconversional method, the activation energy does not remain constant during the reaction process, indicating a complex process. The activation energy is 143.18 ± 2.21, 134.90 ± 4.72, and 128.93 ± 2.41 kJ mol^{-1} for each separated endothermic, LTD, and HTD stage, respectively.
(6) From the mathematical deconvolution results, the kinetic parameters of the thermal decomposition process are evaluated by the kinetics-based simulation approach. The simulation results have a high fitting degree to the experimental data.

Our research reveals the kinetic model of AP, which would contribute to an improved understanding of the AP's

decomposition and should be instrumental for its safe storage and use.

Acknowledgements The authors gratefully acknowledge the National key R&D Program of China (2017YFC0804701-4) and the Scientific and Technological Innovation Programs of Higher Education Institutions in Shanxi (2020L0660) for their financial support.

Declaration

Competing interest The authors declare that they have no known competing financial interests or personal relationships that could have appeared to influence the work reported in this paper.

References

1. Badgujar DM, Talawar MB, Asthana SN. Advances in science and technology of modern energetic materials: an overview. J Hazard Mater. 2008;151:289–305. https://doi.org/10.1016/j.jhazmat.2007.10.039.
2. Singh G, Kapoor IPS, Dubey S. Bimetallic nanoalloys: preparation, characterization and their catalytic activity. J Alloy Compd. 2009;480:270–4. https://doi.org/10.1016/j.jallcom.2009.02.024.
3. Tang G, Tian S-Q, Zhou Z-X. ZnO micro/nanocrystals with tunable exposed (0001) facets for enhanced catalytic activity on the thermal decomposition of ammonium perchlorate. J Phys Chem C. 2014;118:11833–41. https://doi.org/10.1021/jp503510x.
4. Maycock N, Verneker VRP, Rouch L. Influence of growth parameters on the reactivity of ammonium perchlorate. Inorg Nucl Chem Lett. 1968;4:119–23. https://doi.org/10.1016/0020-1650(68)80150-3.
5. Lang AJ, Vyazovkin S. Effect of pressure and sample type on decomposition of ammonium perchlorate. Combust Flame. 2006;145:779–90. https://doi.org/10.1016/j.combustflame.2006.02.002.
6. Zhu Y-L, Huang H, Ren H. Kinetics of thermal decomposition of ammonium perchlorate by TG/DSC-MS-FTIR. J Energ Mater. 2014;32:16–26. https://doi.org/10.1080/07370652.2012.725453.
7. Rajić M, Sućeska M. Study of thermal decomposition kinetics of low-temperature reaction of ammonium perchlorate by isothermal TG. J Therm Anal Calorim. 2001;63:375–86. https://doi.org/10.1023/a:1010136308310.
8. Vyazovkin S, Wight CA. Kinetics of thermal decomposition of cubic ammonium perchlorate. Chem Mater. 1999;11:3386–93. https://doi.org/10.1021/cm9904382.
9. Liu L-L, Li F-S, Tan L-H. Effects of nanometer Ni, Cu, Al and NiCu powders on the thermal decomposition of ammonium perchlorate. Propellants Explos Pyrotech. 2004;29:34–8. https://doi.org/10.1002/prep.200400026.
10. Chen J, He S-M, Huang B. Highly space-confined ammonium perchlorate in three-dimensional hierarchically ordered porous carbon with improved thermal decomposition properties. Appl Surf Sci. 2018;457:508–15. https://doi.org/10.1016/j.apsusc.2018.06.301.
11. Deng P, Wang H-X, Yang X-B. Thermal decomposition and combustion performance of high-energy ammonium perchlorate-based molecular perovskite. J Alloy Compd. 2020;827:154257. https://doi.org/10.1016/j.jallcom.2020.154257.
12. Zhou L-Y, Cao H-B, Zhang L-L. Facet effect of Co_3O_4 nanocatalysts on the catalytic decomposition of ammonium perchlorate. J Hazard Mater. 2020;392: 122358. https://doi.org/10.1016/j.jhazmat.2020.122358.
13. Zou M, Jiang Xi-H, Lu L-D. Nano or micro? A mechanism on thermal decomposition of ammonium perchlorate catalyzed by cobalt oxalate. J Hazard Mater. 2012; 226: 124–30. https://doi.org/10.1016/j.jhazmat.2012.05.010
14. Khairetdinov EF, Boldyrev VV. The mechanism of the low-temperature decomposition of NH_4ClO_4. Thermochim Acta. 1980;41:63–86. https://doi.org/10.1016/0040-6031(80)80096-7.
15. Kiselev AN, Plyusnin VN, Boldyreva AV. Effect of preliminary treatment of ammonium perchlorate by a shock wave on its rate of thermal decomposition and burning of mixtures on its base. Combust Explo Shock. 1972;8:489–91. https://doi.org/10.1007/BF00741211.
16. Sheng M, Valco D, Tucker C. Practical use of differential scanning calorimetry for thermal stability hazard evaluation. Org Process Res Dev. 2019;23:2200–9. https://doi.org/10.1021/acs.oprd.9b00266.
17. Koga N, Goshi Y, Yamada S. Kinetic approach to partially overlapped thermal decomposition processes. J Therm Anal Calorim. 2013;111:1463–74. https://doi.org/10.1007/s10973-012-2500-6.
18. Dolgoborodov AY, Streletskii AN, Shevchenko AA. Thermal decomposition of mechanoactivated ammonium perchlorate. Thermochim Acta. 2018;669:60–5. https://doi.org/10.1016/j.tca.2018.09.007.
19. Hu Y-H, Yang S-M, Tao B-W. Catalytic decomposition of ammonium perchlorate on hollow mesoporous CuO microspheres. Vacuum. 2019;159:105–11.
20. Singh G, Kapoor IPS, Mannan SM. Studies on energetic compounds Part 8: Thermolysis of Salts of HNO_3 and $HClO_4$. J Hazard Mater. 2000;79:1–18. https://doi.org/10.1016/S0304-3894(00)00159-X.
21. Mallick L, Kumar S, Chowdhury A. Thermal decomposition of ammonium perchlorate-A TGA-FTIR-MS study: Part I. Thermochim Acta. 2015;610:57–68. https://doi.org/10.1016/j.tca.2015.04.025.
22. Chaturvedi S, Dave PN. A review on the use of nanometals as catalysts for the thermal decomposition of ammonium perchlorate. J Saudi Chem Soc. 2013;17:135–49. https://doi.org/10.1016/j.jscs.2011.05.009.
23. Kishore K, Verneker VRP, Mohan VK. Differential scanning calorimetric studies on ammonium perchlorate. Thermochim Acta. 1975;13:277–92. https://doi.org/10.1016/0040-6031(75)85048-9.
24. Stoessel F. Thermal safety of chemical processes: risk assessment and process design. Weinheim: WILEY-VCH Verlag GmbH & Co. KGaA; 2008.
25. Jacobs PWM, Whitehead HM. Decomposition and combustion of ammonium perchlorate. Chem Rev. 1969;69:551–90. https://doi.org/10.1021/cr60260a005.
26. Manelis GB, Proshchin AV, Rubtsov YI. Thermal decomposition kinetics of ammonium perchlorate at high temperatures. Combust Explo Shock. 1968;4:169–75. https://doi.org/10.1007/BF00750855.
27. Maycock JN, Verneker VRP. Role of point defects in the thermal decomposition of ammonium perchlorate. P Roy Soc A. 1968;307:303–15. https://doi.org/10.1098/rspa.1968.0191.
28. Vyazovkin S, Burnham AK, Criado JM. ICTAC Kinetics Committee recommendations for performing kinetic computations on thermal analysis data. Thermochim Acta. 2011;520:1–19. https://doi.org/10.1016/j.tca.2011.03.034.
29. Robert AGK, Siegmund F. Thermal decomposition of ammonium perchlorate. Quarterly Rev Chem Soc. 1968;23:430–59. https://doi.org/10.1039/QR9692300430.
30. Mallick L, Kumar S, Chowdhury A. Thermal decomposition of ammonium perchlorate-A TGA-FTIR-MS study: Part II. Thermochim Acta. 2017;653:83–96. https://doi.org/10.1016/j.tca.2017.04.004.

31. Evans MW, Beyer RB, McCulley L. Initiation of deflagration waves at surfaces of ammonium perchlorate-copper chromite-carbon pellets. J Chem Phys. 1964;40:2431–8. https://doi.org/10.1063/1.1725544.
32. Zhu R-S, Lin M-C. Mechanism and kinetics for ammonium perchlorate sublimation: a first-principles study. J Phys Chem C. 2008;112:14481–5. https://doi.org/10.1021/jp803224x.
33. Bircumshaw LL, Newman BH. The thermal decomposition of ammonium perchlorate-I. Introduction, experimental, analysis of gaseous products, and thermal decomposition experiments. P Roy Soc A. 1954; 227:115–132. https://doi.org/10.1098/rspa.1954.0284
34. Boldyrev VV. Thermal decomposition of ammonium perchlorate. Thermochim Acta. 2006;443:1–36. https://doi.org/10.1016/j.tca.2005.11.038.
35. Bircumshaw LL, Newman BH. Thermal decomposition of ammonium perchlorate II. The kinetics of the decomposition, the effect of particle size, and discussion of results. P Roy Soc A. 1955; 227:228–241. https://doi.org/10.1098/rspa.1955.0006
36. Wang H-Y, Jacob RJ, Jeffery B. Assembly and encapsulation of aluminum NP's within AP/NC matrix and their reactive properties. Combust Flame. 2017;180:175–83. https://doi.org/10.1016/j.combustflame.2017.02.036.
37. Vyazovkin S, Burnham AK, Favergeon L. ICTAC Kinetics Committee recommendations for analysis of multi-step kinetics. Thermochim Acta. 2020;689: 178597. https://doi.org/10.1016/j.tca.2020.178597.
38. Perejón A, Pedro ES-J, José MC. Kinetic Analysis of Complex Solid-State Reactions. A New Deconvolution Procedure. J Phys Chem B. 2011; 115: 1780–91.https://doi.org/10.1021/jp110895z.
39. Muravyev NV, Koga N, Meerov DB. Kinetic analysis of overlapping multistep thermal decomposition comprising exothermic and endothermic processes: thermolysis of ammonium dinitramide. Phys Chem Chem Phys. 2017;19:3254–64. https://doi.org/10.1039/c6cp08218a.
40. Yu Q, Liu Y, Sui H, Sun J. Kinetic Analysis of Overlapping Multistep Thermal Decomposition of 2,6-Diamino-3,5-Dinitropyrazine-1-Oxide (LLM-105). J Phys Chem C. 2018;122:25999–6006. https://doi.org/10.1021/acs.jpcc.8b07817.
41. Koga N, Goshi Y, Yamada S. kinetic approach to partially overlapped thermal decomposition processes. J Therm Anal Calorim. 2012;111:1463–74. https://doi.org/10.1007/s10973-012-2500-6.
42. Pedro E. S-, Perejón A, Criado J M. Kinetic model for thermal dehydrochlorination of poly(vinyl chloride). Polymer. 2010; 51:3998–4007. https://doi.org/10.1016/j.polymer.2010.06.020.
43. Kitabayashi S, Koga N. Thermal decomposition of Tin(II) oxyhydroxide and subsequent oxidation in air: kinetic deconvolution of overlapping heterogeneous processes. J Phys Chem C. 2015;119:16188–99. https://doi.org/10.1021/acs.jpcc.5b04975.
44. Eslami A, Hasani N. Thermoanalytical study of linkage isomerism in coordination compounds Part II: Solid state stepwise thermal interconversion of dinitro and dinitrito linkage isomers of trans-bis(ethylenediamine)cobalt(III) hexafluorophosphate. J Therm Anal Calorim. 2013;111:193–201. https://doi.org/10.1007/s10973-012-2470-8.
45. Politzer P, Lane P. Energetics of ammonium perchlorate decomposition steps. J Mol Struct(Theochem). 1998; 454:229–35. https://doi.org/10.1016/S0166-1280(98)00293-0
46. Góbi S, Zhao L, Xu B. A vacuum ultraviolet photoionization study on the thermal decomposition of ammonium perchlorate. Chem Phys Lett. 2018;691:250–7. https://doi.org/10.1016/j.cplett.2017.11.026.
47. Verneker VRP, McCarty M, Maycock JN. Sublimation of ammonium perchlorate. Thermochim Acta. 1971;3:37–48. https://doi.org/10.1016/0040-6031(71)85055-4.
48. Jacobs PWM, Russell-Jones A. Sublimation of ammonium perchlorate. J Phys Chem. 1968;72:202–7. https://doi.org/10.1021/j100847a038.
49. Gilbert R, Jacobs PWM. Thermal decomposition of perchloric acid. Combust Flame. 1971;17:343–53. https://doi.org/10.1016/S0010-2180(71)80056-1.
50. Jacobs PWM, Russell-Jonesthe A. Thermal decomposition and ignition of mixtures of ammonium perchlorate+copper chromite. Symposium (International) on Combustion. 1967;11:457–62. https://doi.org/10.1016/S0082-0784(67)80170-X